



Phase-field model of coupled insulator-metal transitions and oxygen vacancy redox reactionsYin Shi ^{*}, Venkatraman Gopalan, and Long-Qing Chen [†]*Department of Materials Science and Engineering, Materials Research Institute, The Pennsylvania State University, University Park, Pennsylvania 16802, USA*

(Received 2 November 2022; revised 9 April 2023; accepted 28 April 2023; published 15 May 2023)

A predominant ubiquitous feature of strongly correlated oxides is the possible presence of oxygen vacancies, which has recently been shown to have profound effects on their electronic phase transitions. Here, we formulate a comprehensive phase-field model of intercoupled insulator-metal transitions and oxygen vacancy redox reactions, taking into account the valence electron state of oxygen vacancies. We use the model to study the voltage self-oscillation phenomenon in a prototypical strongly correlated oxide, VO₂, and discover the mutual activation of the insulator-metal transition and oxygen vacancy redox reactions leading to systematic enhancement of the oscillation frequency. The established methodology and the mutual activation mechanism are generally applicable to understanding any insulator-metal transition dynamics in oxygen-deficient correlated oxides and improving the performance of voltage self-oscillation-based artificial neurons.

DOI: [10.1103/PhysRevB.107.L201110](https://doi.org/10.1103/PhysRevB.107.L201110)

Strongly correlated oxides are often characterized by the presence of multiple distinct electronic phases that can be manipulated by thermal, mechanical, electrical, magnetic, and photonic stimuli. They have an important ubiquitous feature, the possible presence of oxygen vacancies, which has recently been shown to enable reversible electronic phase transitions on a nanoscale [1–7]. The amount of oxygen vacancies can be controlled not only by chemical doping but also by electric fields [1–4], which is of great relevance to device applications.

While oxygen vacancy migration is generally slow compared to electronic phase transitions, the redox reactions of oxygen vacancies, i.e., the ionization of oxygen vacancies and the recombination of ionized oxygen vacancies with free electrons, are fast and take place concurrently with electronic phase transitions. To our knowledge, there has been no computational model for understanding the coupled electronic phase transitions and oxygen vacancy redox reactions. Therefore, one of the main objectives of this work is to develop a phase-field methodology for such intercoupled electronic phase transitions and oxygen vacancy redox reactions based on our prior works on concurrent insulator-metal and structural phase transitions [8,9]. We distinguish the ionized and neutral oxygen vacancies to allow for the dynamical reactions of oxygen vacancies and charge carriers, taking into account the valence electron state of oxygen vacancies and the low-energy effective band structure of the oxide.

We take the prototypical strongly correlated oxide, VO₂, as an example and study its voltage self-oscillation phenomenon [10–20], which is a manifestation of the nonlinear electronic dynamics of spontaneously repeating insulator-metal

transitions. The voltage self-oscillation is easily realized in compact capacitor-free and inductor-free circuits, which consist of only a VO₂ film connected to a direct bias voltage through a series resistor. It can naturally emulate neural behavior and thus has important potential applications in neuromorphic engineering [21]. We discover that the oxidation (reduction) of oxygen vacancies and the insulator-to-metal (metal-to-insulator) transition activate each other in a positive feedback loop, accelerating both the charge carrier evolution and the insulator-metal transition. We show that this mechanism can systematically increase the voltage self-oscillation frequency, which is highly desirable for neuromorphic computing.

We start with a brief introduction of the existing phase-field model of the noncapacitive phase self-oscillation of VO₂ [22]. It employs a structural order parameter η and a singlet-pairing order parameter ψ to characterize the coupled structural and insulator-metal phase transitions. The evolution of the mesoscale system is governed by the nonequilibrium free energy of the system, which is a functional of all the relevant physical fields, $G = \int g(T(x), \phi(x), \eta(x), \psi(x), n(x), p(x)) dx_1 dx_2 dx_3$, where g is the free energy density, $x \equiv (x_1, x_2, x_3, t)$ the spatiotemporal coordinates, $T(x)$ the temperature field, $\phi(x)$ the electrical potential, $n(x)$ the free electron density field, and $p(x)$ is the free hole density field. The relaxation of the system's state is driven by the thermodynamic driving force that can be computed from the variation of free energy functional with respect to the field variables.

To incorporate oxygen vacancies into the existing model, we add to g the nonequilibrium free energy density of oxygen vacancies, g_{V_O} , as a function of the ionized oxygen vacancy concentration $[V_O^\bullet]$ and the neutral oxygen vacancy concentration $[V_O^\times]$ (see Supplemental Material [23] for the derivation), to form the total free energy, $G_t = \int (g + g_{V_O}) d^3r$. The evolution of ionized and neutral oxygen vacancy concentration

^{*}yxs187@psu.edu[†]lqc3@psu.edu

fields on mesoscale is described by the diffusion-reaction equations,

$$\frac{\partial[V_{\text{O}}^{\cdot\cdot}]}{\partial t} = \nabla \cdot \left(\frac{D[V_{\text{O}}^{\cdot\cdot}]}{k_{\text{B}}T} \nabla \frac{\delta G_{\text{t}}}{\delta[V_{\text{O}}^{\cdot\cdot}]} \right) + S^{\cdot\cdot} - S^{\times}, \quad (1)$$

$$\frac{\partial[V_{\text{O}}^{\times}]}{\partial t} = \nabla \cdot \left(\frac{D[V_{\text{O}}^{\times}]}{k_{\text{B}}T} \nabla \frac{\delta G_{\text{t}}}{\delta[V_{\text{O}}^{\times}]} \right) - S^{\cdot\cdot} + S^{\times}, \quad (2)$$

where D is the diffusion coefficient matrix assumed to be the same for ionized and neutral oxygen vacancies. $S^{\cdot\cdot}$ and S^{\times} are source terms reflecting the redox reactions of oxygen vacancies,

$$V_{\text{O}}^{\times} \rightleftharpoons V_{\text{O}}^{\cdot\cdot} + 2e', \quad (3)$$

$$V_{\text{O}}^{\cdot\cdot} \rightleftharpoons V_{\text{O}}^{\times} + 2h', \quad (4)$$

respectively. The chemical equilibrium constants of reactions (3) and (4) are (see Supplemental Material [23] for the derivation)

$$K^{\cdot\cdot} = N_{\text{c}}^2 \mathcal{F}^2 \left(-\frac{E_{\text{g}}/2 - e\phi - \mu_{\text{eq}}^{\text{e}}}{k_{\text{B}}T} \right) e^{(2\epsilon_{\text{d}} - 2e\phi - 2\mu_{\text{eq}}^{\text{e}})/(k_{\text{B}}T)}, \quad (5)$$

$$K^{\times} = N_{\text{v}}^2 \mathcal{F}^2 \left(-\frac{E_{\text{g}}/2 + e\phi + \mu_{\text{eq}}^{\text{e}}}{k_{\text{B}}T} \right) e^{(-2\epsilon_{\text{d}} + 2e\phi + 2\mu_{\text{eq}}^{\text{e}})/(k_{\text{B}}T)}, \quad (6)$$

respectively. Here N_{c} and N_{v} are the effective densities of states of the conduction and valence bands, respectively. $E_{\text{g}} = E_{\text{g}0}\psi^2$ as a function of the electronic order parameter is the energy gap where $E_{\text{g}0}$ is the gap of the insulating M1 phase (at the transition temperature). e is the magnitude of the elementary charge and k_{B} is the Boltzmann constant. $\mu_{\text{eq}}^{\text{e}}$ is the electron chemical potential at equilibrium. $\mathcal{F}(\cdot)$ is the Fermi integral of order 1/2 which can be approximated to an analytical function [24]. ϵ_{d} is the defect level. Then we can write down the source terms (see Supplemental Material [23] for a detailed description),

$$S^{\cdot\cdot} = \alpha^{\cdot\cdot} (K^{\cdot\cdot} [V_{\text{O}}^{\times}] - [V_{\text{O}}^{\cdot\cdot}] n^2), \quad (7)$$

$$S^{\times} = \alpha^{\times} (K^{\times} [V_{\text{O}}^{\cdot\cdot}] - [V_{\text{O}}^{\times}] p^2), \quad (8)$$

where $\alpha^{\cdot\cdot}$ and α^{\times} are prefactors. The redox reactions of oxygen vacancies (3) and (4) generate or eliminate charge carriers so they also add source terms $2S^{\cdot\cdot}$ and $2S^{\times}$ to the diffusion-reaction equations of free electrons and free holes, respectively. The Gauss law for the electrical potential should include the charge density from ionized oxygen vacancies, $+2[V_{\text{O}}^{\cdot\cdot}]$, into the total charge density.

The parameter values used in the simulations are described in the Supplemental Material [23] (see also Ref. [25] therein). It is noted that compared to their redox reactions, oxygen vacancies migrate much more slowly and could barely move within milliseconds, so their (electro-) migration should not be an underlying mechanism of any phenomena observed in this study (only focusing on evolution within 1 μs).

We use the finite element method implemented in the FEniCS open-source C++ library [26–28] to solve the equations of evolution [22] including Eqs. (1) and (2). The boundary conditions for Eqs. (1) and (2) are the Neumann condition with zero flux, meaning the total number of oxygen vacancies in the system is conserved. The initial distribution

of oxygen vacancies is homogeneous. Other details of solving the equations of evolution were summarized in Ref. [22].

Figure 1(a) is a schematic of the system we are simulating. A VO_2 thin film is in series connection with a resistor R_{s} for limiting the current and is supplied with a direct bias voltage V_{b} . The voltage drop across the film V can self-oscillate for certain ranges of V_{b} and R_{s} , which is indicated by the voltage waveform monitored by the oscilloscope. The film contains oxygen vacancies so it is formally $\text{VO}_{2-\delta}$ with δ being the concentration of oxygen vacancies measured per formula unit (f.u.). Other details of the system were presented in Ref. [22].

Figure 1(b) shows the voltage self-oscillation frequency f as a function of the oxygen vacancy concentration δ at different pairs of the bias voltage and series resistance. δ is tuned by the variation of $\mu_{\text{eq}}^{\text{e}}$. First, for all pairs of V_{b} and R_{s} , the frequency increases as oxygen vacancies are gradually introduced into VO_2 and then it decreases a bit until the voltage self-oscillation ceases. The frequency reaches a maximum of 27.3 MHz for $V_{\text{b}} = 9$ V and $R_{\text{s}} = 500$ k Ω , which is a 39% enhancement compared to the frequency in the absence of oxygen vacancies, 19.64 MHz [22]. Second, the frequency curves as functions of the oxygen vacancy concentration for the same $V_{\text{b}}/R_{\text{s}}$ ratio are almost identical, while the curve for a smaller $V_{\text{b}}/R_{\text{s}}$ ratio climbs up more steeply.

We then examine how the frequency changes with respect to the defect level ϵ_{d} . Although the defect level of oxygen vacancies in VO_2 is fixed, varying ϵ_{d} can be thought of as doping VO_2 with different donors. This will provide useful insights into the strategy of choosing donors to maximally promote the voltage self-oscillation frequency. Figure 1(c) shows the frequency and oxygen vacancy concentration as functions of the defect level. As ϵ_{d} increases to the conduction band bottom, the frequency increases monotonically until it reaches a saturation value of 28.5 MHz, meanwhile δ decreases monotonically. The frequency saturates effectively at $\epsilon_{\text{d}}/E_{\text{g}0} \approx 0.3$. The saturation frequency is higher than the maximal frequency achieved with $\epsilon_{\text{d}}/E_{\text{g}0} = 0.14$ for oxygen vacancies, indicating that a donor with a shallower defect level tends to enhance the frequency more strongly.

Figure 2 shows the self-oscillation waveforms of the concentrations of ionized and neutral oxygen vacancies averaged over the $\text{VO}_{2-\delta}$ film. It has been shown that during the voltage self-oscillation, not the whole film but only a filament [nucleated at the defect region; see Fig. 1(a)] switches between the insulating and metallic states [22]. Therefore, the changes in these concentrations are localized in the conductive filament. This is actually an example of oscillating chemical reactions [29], which is driven by and interacts with the insulator-metal transition of the host material.

The mechanism of the frequency enhancement due to oxygen vacancies can be understood from the chemical equilibrium constants (5) and (6), which reflect the rates of the redox reactions of oxygen vacancies (3) and (4). The redox reactions impose driving forces $2S^{\cdot\cdot}$ and $2S^{\times}$ to the evolution of the free electron density n and free hole density p , respectively. This is the origin of why the state evolution could be accelerated by the introduction of oxygen vacancies, which underlines the importance of taking into account the dynamic ionization of defects for such nonequilibrium phenomena in

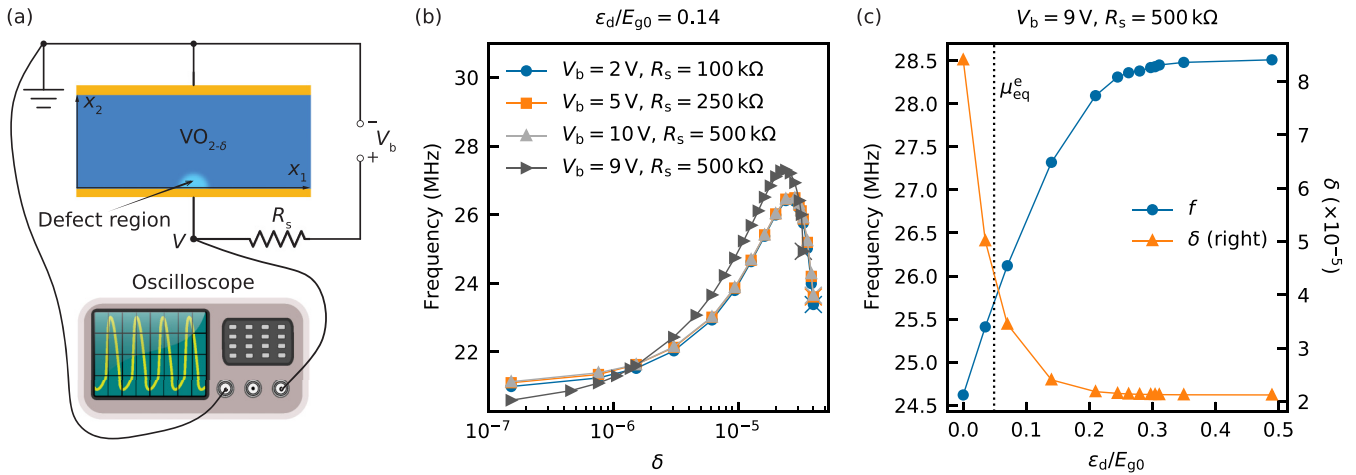


FIG. 1. Enhancement of the voltage self-oscillation frequency due to the presence of oxygen vacancies. (a) A schematic of the system. The defect region is a metallic phase nucleation site with an effectively lower transition temperature to imitate the realistic situation where the first-order insulator-metal transition always starts from localized nucleation sites. (b) Frequency as a function of the oxygen vacancy concentration at various bias voltages and series resistances. The crosses mark the termination of the voltage self-oscillation. Throughout this work, the defect level and chemical potentials are all measured from the midpoint of the energy gap. (c) Frequency and oxygen vacancy concentration as functions of the defect level. The black dotted vertical line marks the equilibrium chemical potential of free electrons.

strongly correlated materials. Figure 3 presents the chemical equilibrium constants as functions of the conduction band bottom $E_c = E_g/2$ (measured from the midpoint of the gap), equilibrium chemical potential of free electrons, and defect level. As E_c decreases, i.e., the gap closes, $K^{\cdot\cdot}$ dramatically increases after E_c passes the defect level, meanwhile K^{\times} remains small although it also increases. This means that the insulator-metal transition activates the oxidation of oxygen vacancies, which suddenly releases many additional free

electrons. An intuitive way of interpreting this is that as E_c becomes lower than ϵ_d , the defect level is suddenly in the conduction band thereby freeing all electrons on it. Mathematically speaking, the activation of the ionization induces a large driving force for the evolution of n . The resulting faster evolution of n in turn accelerates the phase transition itself because additional charge carriers are known to assist the collapse of the energy gap [30], a collective effect that has been naturally accounted for in the phase-field model [9,22,31]. This procedure is thus an avalanche process, resulting in the enhancement of the operation frequency of the voltage self-oscillation.

The middle panel of Fig. 3 shows weak dependence of $K^{\cdot\cdot}$ and K^{\times} on μ_{eq}^e . On the other hand, an increase in μ_{eq}^e will lead to an exponential increase in the neutral oxygen vacancy concentration at equilibrium, so more electrons will be released as the gap closes, promoting the frequency.

The monotonic increase in the frequency as ϵ_d increases [Fig. 1(c)] is counterintuitive at the first glance because the shallower the defect level is, the less neutral oxygen vacancies are left as a reservoir of electrons. However, increasing ϵ_d has another effect which is to enhance the reaction rate of the ionization of oxygen vacancies, reaction (3). This can be seen clearly through the pure exponential dependence of $K^{\cdot\cdot}$ on ϵ_d as in Eq. (5) and the right panel of Fig. 3, and it reflects the decreasing activation energy for the ionization of oxygen vacancies. These two effects combined eventually lead to the increase in the frequency. To explain it quantitatively, we plot in the right panel of Fig. 3 the quantity $S^{\cdot\cdot}/\alpha^{\cdot\cdot}$ [see Eq. (7)] as a function of ϵ_d but at a fixed E_c and μ_{eq}^e (marked by vertical lines) and a quasichemical potential of neutral oxygen vacancies $\mu^{\times} = \epsilon_f - \mu_{eq}^e$ with charge neutrality, where ϵ_f is the formation energy of a $V_{O}^{\cdot\cdot}$. $S^{\cdot\cdot}/\alpha^{\cdot\cdot}$ is proportional to the rate of the ionization of oxygen vacancies at the given

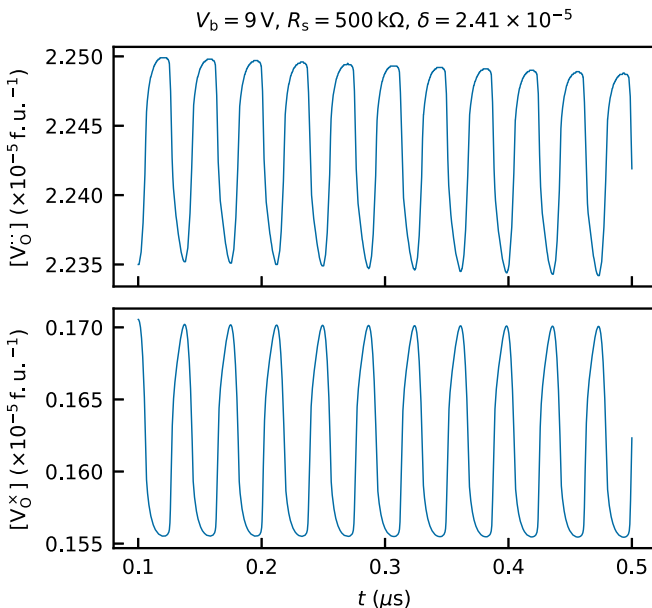


FIG. 2. Self-oscillation waveforms of the ionized oxygen vacancy concentration (upper panel) and neutral oxygen vacancy concentration (lower panel) averaged over the film.

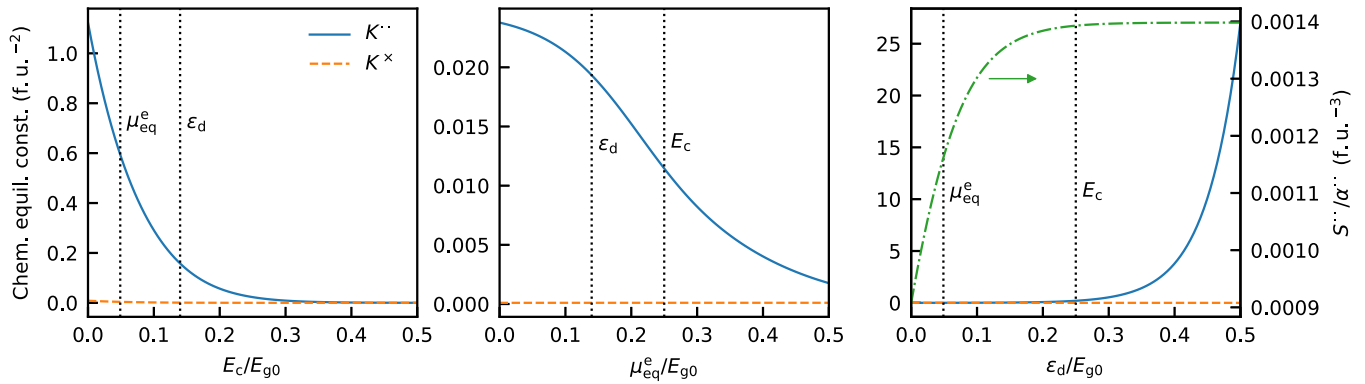


FIG. 3. Chemical equilibrium constants of the redox reactions of oxygen vacancies at $\phi = 0$, as functions of the conduction band bottom E_c (left panel), equilibrium electron chemical potential (middle panel), and defect level (right panel), respectively. In the right panel, we also plot to the right y axis the quantity $S^{\cdot\cdot}/\alpha^{\cdot\cdot}$ proportional to the rate of the ionization of oxygen vacancies (see text). The fixed quantities are marked by black dotted vertical lines.

moment marked by E_c and μ^{\times} . Indeed, $S^{\cdot\cdot}/\alpha^{\cdot\cdot}$ increases as ϵ_d increases and it saturates near $\epsilon_d/E_{g0} = 0.25$, which is the precise reason for the monotonic increase and early saturation of the frequency with increasing ϵ_d [Fig. 1(c)].

In conclusion, we developed a phase-field model of intercoupled insulator-metal transitions and oxygen vacancy redox reactions. By investigating the voltage self-oscillation in the prototypical correlated oxide, VO_2 , we predicted a self-oscillating redox reaction of oxygen vacancies and found that the insulator-metal transition and oxygen vacancy redox reactions mutually promote each other, leading to $\sim 40\%$

enhancement in the operation frequency compared to the pristine case. The established methodology and discovered mechanism are general because they are based only on the fundamental irreversible thermodynamics and the universal property (charge-carrier induced melting of the localized state) of Mott transitions.

This work was supported as part of the Computational Materials Sciences Program funded by the U.S. Department of Energy, Office of Science, Basic Energy Sciences, under Award No. DE-SC0020145.

- [1] J. Jeong, N. Aetukuri, T. Graf, T. D. Schladt, M. G. Samant, and S. S. P. Parkin, Suppression of metal-insulator transition in VO_2 by electric field-induced oxygen vacancy formation, *Science* **339**, 1402 (2013).
- [2] J. Jeong, N. B. Aetukuri, D. Passarello, S. D. Conradson, M. G. Samant, and S. S. P. Parkin, Giant reversible, facet-dependent, structural changes in a correlated-electron insulator induced by ionic liquid gating, *Proc. Natl. Acad. Sci. USA* **112**, 1013 (2015).
- [3] Y. Sharma, J. Balachandran, C. Sohn, J. T. Krogel, P. Ganesh, L. Collins, A. V. Ievlev, Q. Li, X. Gao, N. Balke, O. S. Ovchinnikova, S. V. Kalinin, O. Heinonen, and H. N. Lee, Nanoscale control of oxygen defects and metal-insulator transition in epitaxial vanadium dioxides, *ACS Nano* **12**, 7159 (2018).
- [4] D. Schrecongost, M. Aziziha, H.-T. Zhang, I.-C. Tung, J. Tessmer, W. Dai, Q. Wang, R. Engel-Herbert, H. Wen, Y. N. Picard, and C. Cen, On-demand nanoscale manipulations of correlated oxide phases, *Adv. Funct. Mater.* **29**, 1905585 (2019).
- [5] Q. Lu, C. Sohn, G. Hu, X. Gao, M. F. Chisholm, I. Kylänpää, J. T. Krogel, P. R. C. Kent, O. Heinonen, P. Ganesh, and H. N. Lee, Metal-insulator transition tuned by oxygen vacancy migration across TiO_2/VO_2 interface, *Sci. Rep.* **10**, 18554 (2020).
- [6] J. Li, R. J. Green, Z. Zhang, R. Sutarto, J. T. Sadowski, Z. Zhu, G. Zhang, D. Zhou, Y. Sun, F. He, S. Ramanathan, and R. Comin, Sudden Collapse of Magnetic Order in Oxygen-Deficient Nickelate Films, *Phys. Rev. Lett.* **126**, 187602 (2021).
- [7] Q. Zhang, G. Hu, V. Starchenko, G. Wan, E. M. Dufresne, Y. Dong, H. Liu, H. Zhou, H. Jeon, K. Saritas, J. T. Krogel, F. A. Reboredo, H. N. Lee, A. R. Sandy, I. C. Almazan, P. Ganesh, and D. D. Fong, Phase Transition Dynamics in a Complex Oxide Heterostructure, *Phys. Rev. Lett.* **129**, 235701 (2022).
- [8] Y. Shi, F. Xue, and L.-Q. Chen, Ginzburg-Landau theory of metal-insulator transition in VO_2 : The electronic degrees of freedom, *Europhys. Lett.* **120**, 46003 (2017).
- [9] Y. Shi and L.-Q. Chen, Current-Driven Insulator-to-Metal Transition in Strongly Correlated VO_2 , *Phys. Rev. Appl.* **11**, 014059 (2019).
- [10] Y. W. Lee, B.-J. Kim, J.-W. Lim, S. J. Yun, S. Choi, B.-G. Chae, G. Kim, and H.-T. Kim, Metal-insulator transition-induced electrical oscillation in vanadium dioxide thin film, *Appl. Phys. Lett.* **92**, 162903 (2008).
- [11] H.-T. Kim, B.-J. Kim, S. Choi, B.-G. Chae, Y. W. Lee, T. Driscoll, M. M. Qazilbash, and D. N. Basov, Electrical oscillations induced by the metal-insulator transition in VO_2 , *J. Appl. Phys.* **107**, 023702 (2010).
- [12] M. Pattanayak, M. N. F. Hoque, Y. Zhao, Z. Fan, and A. A. Bernussi, Tunable VO_2 relaxation oscillators for analog applications, *Semicond. Sci. Technol.* **34**, 105028 (2019).
- [13] J. Sakai, High-efficiency voltage oscillation in VO_2 planer-type junctions with infinite negative differential resistance, *J. Appl. Phys.* **103**, 103708 (2008).

- [14] Y. Wang, J. Chai, S. Wang, L. Qi, Y. Yang, Y. Xu, H. Tanaka, and Y. Wu, Electrical oscillation in Pt/VO₂ bilayer strips, *J. Appl. Phys.* **117**, 064502 (2015).
- [15] D. Lepage and M. Chaker, Thermodynamics of self-oscillations in VO₂ for spiking solid-state neurons, *AIP Adv.* **7**, 055203 (2017).
- [16] S. G. Bortnikov, V. S. Aliev, I. A. Badmaeva, and I. V. Mzhelskiy, VO₂ film temperature dynamics at low-frequency current self-oscillations, *J. Appl. Phys.* **123**, 075701 (2018).
- [17] A. Velichko, M. Belyaev, V. Putrolaynen, V. Perminov, and A. Pergament, Modeling of thermal coupling in VO₂-based oscillatory neural networks, *Solid-State Electron.* **139**, 8 (2018).
- [18] A. Velichko, M. Belyaev, V. Putrolaynen, V. Perminov, and A. Pergament, Thermal coupling and effect of subharmonic synchronization in a system of two VO₂ based oscillators, *Solid-State Electron.* **141**, 40 (2018).
- [19] E. Corti, B. Gotsmann, K. Moselund, A. M. Ionescu, J. Robertson, and S. Karg, Scaled resistively-coupled VO₂ oscillators for neuromorphic computing, *Solid-State Electron.* **168**, 107729 (2020), special issue of Solid-State Electronics, dedicated to EUROSOL-ULIS 2019.
- [20] R. Tobe, M. S. Mian, and K. Okimura, Coupled oscillations of VO₂-based layered structures: Experiment and simulation approach, *J. Appl. Phys.* **127**, 195103 (2020).
- [21] N. Shukla, A. Parihar, E. Freeman, H. Paik, G. Stone, V. Narayanan, H. Wen, Z. Cai, V. Gopalan, R. Engel-Herbert *et al.*, Synchronized charge oscillations in correlated electron systems, *Sci. Rep.* **4**, 4964 (2014).
- [22] Y. Shi and L.-Q. Chen, Intrinsic Insulator-Metal Phase Oscillations, *Phys. Rev. Appl.* **17**, 014042 (2022).
- [23] See Supplemental Material at <http://link.aps.org/supplemental/10.1103/PhysRevB.107.L201110> for a detailed formulation of the model and the parameter values used in the simulations.
- [24] A. N. Morozovska, E. A. Eliseev, O. V. Varenyk, Y. Kim, E. Strelcov, A. Tselev, N. V. Morozovsky, and S. V. Kalinin, Nonlinear space charge dynamics in mixed ionic-electronic conductors: Resistive switching and ferroelectric-like hysteresis of electromechanical response, *J. Appl. Phys.* **116**, 066808 (2014).
- [25] P. P. Boriskov, M. A. Belyaev, and A. A. Velichko, Activation diffusion of oxygen under conditions of the metal-semiconductor phase transition in vanadium dioxide, *Russ. J. Phys. Chem. A* **91**, 1064 (2017).
- [26] M. Alnæs, J. Blechta, J. Hake, A. Johansson, B. Kehlet, A. Logg, C. Richardson, J. Ring, M. E. Rognes, and G. N. Wells, The fenics project version 1.5, *Arch. Numer. Softw.* **3**, 9 (2015).
- [27] A. Logg, K.-A. Mardal, and G. Wells, *Automated Solution of Differential Equations by the Finite Element Method: The FEniCS Book* (Springer Science & Business Media, New York, 2012), Vol. 84.
- [28] A. Logg and G. N. Wells, Dolfin: Automated finite element computing, *ACM Trans. Math. Softw.* **37**, 1 (2010).
- [29] I. R. Epstein and J. A. Pojman, *An Introduction to Nonlinear Chemical Dynamics: Oscillations, Waves, Patterns, and Chaos* (Oxford University Press, Oxford, New York, 1998).
- [30] D. Wegkamp, M. Herzog, L. Xian, M. Gatti, P. Cudazzo, C. L. McGahan, R. E. Marvel, R. F. Haglund, A. Rubio, M. Wolf, and J. Stähler, Instantaneous Band Gap Collapse in Photoexcited Monoclinic VO₂ due to Photocarrier Doping, *Phys. Rev. Lett.* **113**, 216401 (2014).
- [31] Y. Shi, A. E. Duwel, D. M. Callahan, Y. Sun, F. A. Hong, H. Padmanabhan, V. Gopalan, R. Engel-Herbert, S. Ramanathan, and L.-Q. Chen, Dynamics of voltage-driven oscillating insulator-metal transitions, *Phys. Rev. B* **104**, 064308 (2021).